

Brillouin spectrometer interfaced with synchrotron radiation for simultaneous x-ray density and acoustic velocity measurements

Stanislav Sinogeikin^{a)}

Department of Geology, University of Illinois at Urbana-Champaign, Urbana, Illinois 61801 and HPCAT, Carnegie Institution of Washington, Argonne, Illinois 60439

Jay Bass

Department of Geology, University of Illinois at Urbana-Champaign, Urbana, Illinois 61801

Vitali Prakapenka

GSECARS, University of Chicago, Chicago, Illinois 60637

Dmitry Lakshtanov

Department of Geology, University of Illinois at Urbana-Champaign, Urbana, Illinois 61801

Guoyin Shen

HPCAT, Carnegie Institution of Washington, Argonne, Illinois 60439 and GSECARS, University of Chicago, Chicago, Illinois 60637

Carmen Sanchez-Valle

Department of Geology, University of Illinois at Urbana-Champaign, Urbana, Illinois 61801

Mark Rivers

GSECARS, University of Chicago, Chicago, Illinois 60637

(Received 30 June 2006; accepted 11 September 2006; published online 27 October 2006)

We describe a new Brillouin spectrometer that has been installed on a synchrotron x-ray beamline for simultaneous measurements of sound velocities (by Brillouin scattering) and density (by x-ray diffraction). The spectrometer was installed at the 13-BM-D station (GSECARS) of the Advanced Photon Source. This unique facility has been tested in studies of transparent single crystal and polycrystalline materials at high pressure and temperature. The equation of state, acoustic velocities, and, hence, elastic moduli of materials as a function of pressure and temperature can now be determined without resort to a secondary pressure standard, such as the ruby fluorescence scale, or the equation of state of standard materials such as Au, Pt, or MgO, thus offering the potential to determine an absolute pressure scale. This article describes the design of the combined Brillouin-x-ray system and the first experimental results obtained. As a general-user facility, the system was designed to require minimal setup time and alignment of sensitive optics, run-time control and adjustments of optics from outside the experimental station, compatibility with powder and single crystal x-ray diffraction measurements, and no interference with other experimental techniques used on the beamline. To satisfy these requirements we adopted a novel optical design for the Brillouin system with a vertical scattering plane. Examples of measurements of acoustic velocities and elastic moduli on single crystal NaCl (B1) and polycrystalline NaCl (B2) at high pressure and single crystal velocities and elastic moduli of MgO at high temperature (to 600 °C) and at high pressure are presented. © 2006 American Institute of Physics.

[DOI: [10.1063/1.2360884](https://doi.org/10.1063/1.2360884)]

I. INTRODUCTION

Recent advances in high-pressure mineral physics and the development of diamond anvil cell (DAC) techniques allow measurements of lattice parameters by x-ray diffraction (see, e.g., Refs. 1 and 2) and acoustic velocities by Brillouin spectroscopy (see, e.g., Ref. 3) at megabar pressures. A prevailing problem with separate measurements by these techniques is in pressure uncertainty: x-ray measurements must often rely on the equations of state (EOS) of “standard”

materials (Au, Pt, NaCl) for pressure determination, whereas optical experiments typically employ the ruby fluorescence technique.⁴ Regardless of how pressure is measured, different pressure standards generally do not yield identical pressures at the same experimental conditions. The differences in pressure scales introduce considerable uncertainty in determination of the pressure dependence of physical properties. This problem is amplified for measurements under high-temperature–high-pressure conditions.

Simultaneous velocity (e.g., by Brillouin scattering) and density (by x-ray diffraction) measurements at high pressure and temperature result in a complete set of thermoelastic parameters such as isotropic acoustic velocities, adiabatic

^{a)} Author to whom correspondence should be addressed; electronic mail: ssinog@hpcat.aps.anl.gov

and isothermal elastic moduli, their pressure, temperature, and cross P - T derivatives, thermal expansion, and Grüneisen parameter as a function of pressure and temperature. Moreover, simultaneous density and sound velocity measurements allow the accurate determination of an absolute pressure scale, so that the equation of state and velocities of materials as a function of pressure can be determined without resort to a secondary pressure standard (see, e.g., Ref. 5).

Simultaneous velocity and density measurements can now be performed in large volume high-pressure devices by ultrasonic techniques (see, e.g., Refs. 6 and 7). However, such measurements are limited in pressure (<30 GPa) compared with the DAC and are most readily performed on polycrystalline samples, thus providing only limited information on the elastic properties of materials.

One of the advantages of using Brillouin scattering for velocity measurements is that it can be used at extremely high pressures into the megabar range with the diamond anvil cell, and that it offers the opportunity for measurements at simultaneous high pressure and temperature via laser heating (see, e.g., Ref. 8) or resistance heating (see, e.g., Ref. 9). Both single crystal and polycrystalline samples can be measured, and the sample size requirements are very modest.

Here we describe a Brillouin system recently installed and tested at the 13-BM-D experimental station (GSECARS) of the Advanced Photon Source at the Argonne National Laboratory. This is the first Brillouin system interfaced with a synchrotron radiation facility for simultaneous x-ray diffraction and velocity measurements. Because this facility is open to a broad community and must share space with other types of experiments, the design of the Brillouin spectrometer was guided by the following key considerations.

- (1) There should be quick setup, alignment, and breakdown of Brillouin experiments to minimize loss of valuable beam time.
- (2) There should be a complete run-time remote control of optics and electronics for data collection from outside the experimental station.
- (3) The Brillouin spectrometer should be flexible with respect to sample position and compatible with both powder and single crystal diffraction techniques.
- (4) The spectrometer should operate in at least two easily interchangeable symmetric scattering geometries—e.g., 50° and 80°. Smaller scattering angles allow the use of piston-cylinder diamond anvil cells for higher pressures at the expense of slightly increased experimental uncertainty and lower resolution.
- (5) The spectrometer should be compact due to limited space in the beamline station.
- (6) The spectrometer should not interfere with other experimental techniques used on the beamline.
- (7) The complete system should satisfy all laser safety requirements for a class IV laser.

To satisfy these requirements we have adopted a novel optical design that allows one to easily bring the Brillouin optics into place while not requiring frequent alignment of the sensitive spectrometer optics. Most of the Brillouin system is on an elevated optical table so that it does not interfere

with other x-ray experiments. In contrast to a majority of Brillouin systems, we use a vertical scattering plane. This design allows the focusing and collecting optics that are near the sample during an experiment to be easily moved in and out of position for Brillouin work. This article describes the new Brillouin spectrometer at GSECARS, APS, along with several examples of measurements that were performed on single crystal and polycrystalline samples.

II. BRILLOUIN SPECTROSCOPY

A. General considerations

Brillouin scattering results from the inelastic scattering of incident light (photons) from thermally generated acoustic phonons (density and refractive index fluctuations that propagate with the speed of sound). The Brillouin portion of the light scattered by a sample is shifted in frequency with respect to the incident light, with the shift proportional to the velocity of the acoustic waves (see, e.g., Ref. 10):

$$V_i = \left(\frac{\Delta\omega_i}{\omega} \right) \left(\frac{c}{2n \sin(\theta/2)} \right) = \frac{\Delta\omega_i \lambda}{2n \sin(\theta/2)}, \quad (1)$$

where V_i is the velocity of an acoustic wave (subscript i stands for a compressional or one of the shear modes), $\Delta\omega_i$ is the frequency shift of scattered light, ω is the frequency, λ is the wavelength of the incident light, c is the speed of light in vacuum, n is the index of refraction of the sample, and θ is the scattering angle, or the angle between the incident laser ray and scattered ray inside the sample.

Brillouin scattering requires only small transparent or translucent samples that are larger than the focused laser beam (samples with dimensions of $50 \times 50 \times 10 \mu\text{m}^3$ or smaller). Thus, Brillouin scattering experiments are readily combined with the DAC to obtain high-pressure and high-temperature data.^{9,11,12}

Unlike Raman and some other types of spectroscopy, the results of Brillouin spectroscopy are very sensitive to the scattering angle [Eq. (1)]. In addition, most crystalline materials exhibit elastic anisotropy, with different acoustic velocities in different crystallographic directions. Thus, the scattering angle and phonon direction (for single crystals) must be carefully controlled in any experiment. In general, one must know the orientation of the sample crystallographic axes, crystal faces, and optical indicatrix to determine the acoustic velocity and corresponding phonon direction. For practical purposes it is more convenient to use a special “platelet” symmetrical geometry¹³ in which a platelike sample with two flat parallel faces is oriented symmetrically with respect to the incident and scattered light directions (Fig. 1). In this geometry the phonon direction, q , is in the plane of the sample. For the case of an optically isotropic material, Snell’s law $n \sin(\theta/2)$ reduces to $n_0 \sin(\theta^*/2)$ in Eq. (1), where θ^* is the predefined external scattering angle and n_0 is the refractive index of air ($n=1$). In this case the acoustic velocity is simply proportional to the Brillouin shift [$V_i = \lambda \Delta\omega_i / 2 \sin(\theta^*/2)$]. The main advantage of the platelet symmetric geometry is that velocities are measured independent of the sample refractive index (which can change appreciably with temperature, pressure, and across phase transi-

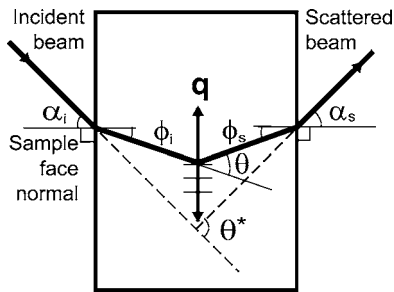


FIG. 1. Platelet, or symmetric, scattering geometry (view normal to scattering plane). The solid lines indicate directions of the incident and scattered beams in the sample (rectangle). α and ϕ are the angles between the incident (i) and scattered (s) beams and sample face normals. q is the phonon direction. θ is the actual scattering angle, and θ^* is the external scattering angle.

tions). This geometry is especially advantageous when the sample is mounted inside a high-pressure (e.g., DAC) (Fig. 2) and/or high-temperature device.^{12,13}

B. Elastic moduli

Isotropic acoustic velocities are directly related to the adiabatic bulk (K_S) and shear (μ) moduli through the equations $\mu = \rho V_S^2$ and $K_S = \rho V_P^2 - (4/3)\mu$ (where V_S is the transverse sound velocity and V_P is the longitudinal velocity). Thus, in elastically isotropic materials (glasses, liquids) and well-sintered polycrystalline materials with proper grain size the aggregate acoustic velocities and elastic moduli (with known density) can be measured directly (see, e.g., Refs. 14 and 15).

In general, acoustic velocities in crystals vary with crystallographic direction. The velocities of acoustic phonons are related to the adiabatic single crystal elastic moduli and density of a material through Christoffel's equation:¹⁶

$$|C_{ijkl}q_jq_l - \rho V^2 \delta_{ik}| = 0, \quad (2)$$

where V is the phonon phase velocity, q_j and q_l are unit vectors in the phonon propagation direction, C_{ijkl} is the elasticity tensor for the material, ρ is the density, and δ_{ik} is the

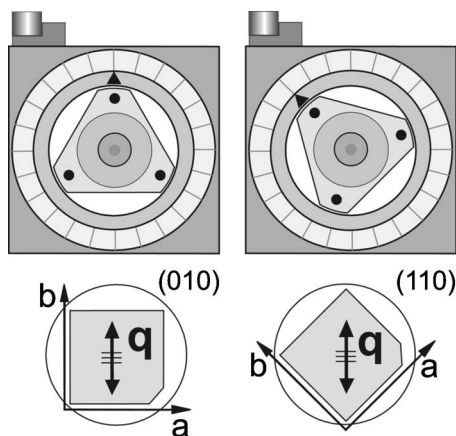


FIG. 2. Velocity measurements in platelet symmetric scattering geometry (view down the sample normal/DAC axis, lying within the scattering plane). The sampled phonon direction in our setup is always vertical. Rotation of the DAC sample around the horizontal sample normal/DAC axis allows measuring acoustic velocities in any crystallographic direction within the sample plane.

Kronecker delta function. Using Eq. (2) the measured acoustic velocities in known crystallographic directions can be inverted to obtain the single crystal elastic moduli using, for example, a linearized general least-squares inversion procedure.¹⁷

The minimum number of crystallographic directions in which velocities need to be measured to obtain the complete elasticity tensor depends on the crystal class of the measured material. For example, cubic materials (e.g., MgO and NaCl) are characterized by three independent elastic moduli and require measurements of longitudinal and transverse acoustic velocities in two distinct crystallographic directions, whereas orthorhombic crystals with nine independent single crystal elastic moduli generally require velocity measurements in a minimum of six directions. The platelet symmetric geometry has the advantage that velocities can be measured in any crystallographic direction within a sample plane by simply rotating the sample around the sample face normal. Thus the complete elastic tensor can be obtained from velocity measurements in a single platelet sample with symmetry as low as orthorhombic.¹¹

Because x-ray density and Brillouin velocity measurements can be readily performed in diamond anvil cells or other high-pressure/high-temperature devices with sufficient optical and x-ray access, the combination of these techniques makes a broad range of high pressures and temperatures accessible for measurements of thermoelastic parameters. This includes single crystal and aggregate adiabatic elastic moduli and their pressure, temperature, and cross derivatives, the isothermal bulk modulus [$K_T = -V(\partial P / \partial V)_T$] and its pressure, temperature, and cross derivatives, temperature-dependent thermal expansion [$\alpha = 1/V(\partial V / \partial P)$], and other parameters such as a thermodynamic Grüneisen parameter (γ). Acoustic velocities are related to adiabatic elastic moduli (K_S and μ), whereas x-ray static compression measurements provide isothermal bulk modulus (K_T). K_S and K_T are related through the relations $K_S = K_T(1 + \alpha\gamma T)$. Thus, simultaneous measurements of density and velocities at high pressure and temperature give an additional benefit of obtaining an absolute pressure without any resort to external pressure markers (see, e.g., Ref. 5).

III. X-RAY

The Brillouin system was installed in the end station 13-BM-D of the bending-magnet beamline. This station is multifunctional and accommodates a large volume press and a lift table that shares the DAC setup with other techniques such as microtomography, microprobe, and extended x-ray-absorption fine structure (EXAFS). A more detailed description of 13-BM-D station can be found in Ref. 18.

The lift table in 13-BM-D consists of two tiers. The main (lower lever) tier is a rectangular optical table (4×6 ft.²) on which the DAC positioning stages and related x-ray equipment are set up (Fig. 3). The upper tier contains the main equipment of the Brillouin system (laser, Fabry-Pérot interferometer, and the majority of optics). The collecting and focusing assemblies of the Brillouin spectrometer are mounted to the bottom of the upper tier table.

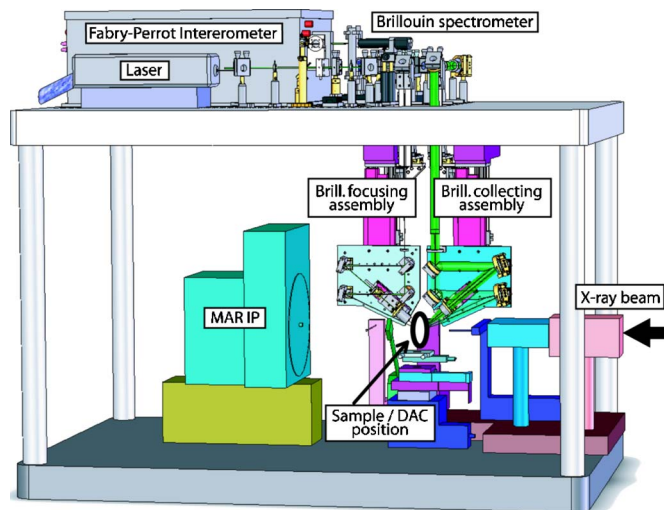


FIG. 3. (Color online) A schematic view of the Brillouin spectroscopy system integrated with the diffraction setup in 13-BM-D.

Beamline 13-BM-D includes a high-energy monochromator, which provides x rays with a variable energy in the range of 5–75 keV. The flux on the sample in DAC experiments is increased by focusing the x-ray beam with Kirpatrick-Baez (KB) mirrors to a $7 \times 20 \mu\text{m}^2$ focal spot at the sample position. The sample positioning assembly is aligned in such a way that when rotating a DAC around the vertical axis (ω circle) the sample always stays in the focus of the x ray at the same distance from the imaging plate. This condition is especially critical for single crystal x-ray measurements with the DAC, when the sample is typically rotated around the vertical axis to obtain a single crystal diffraction pattern.

An imaging plate (IP) system (MAR345) is used as a primary area detector for its large size and high dynamic range. With Brillouin optics in place, the maximum 2θ angle for x-ray diffraction is 30° . In DAC experiments a typical exposure time ranges from 1 to 30 min for powder (polycrystalline) samples (typically 2–5 min for a high-quality image) and is less than 2 min (typically 15–40 s) for single crystal diffraction studies.

IV. BRILLOUIN SPECTROMETER

Brillouin spectrometers usually employ a horizontal scattering plane (the plane containing the incident and scattered light directions), where the incident laser and signal collection paths are parallel to the plane of an optic table (see, e.g., Refs. 11, 17, and 19–21). This provides relatively easy alignment and stability of optical components.

When combining x-ray diffraction with a focused x-ray beam and Brillouin spectroscopy, the position and orientation of the DAC are determined by the direction and focus of the x-ray beam, and the Brillouin system has to be flexible with respect to the sample so it can both deliver a focused laser beam to and collect a Brillouin signal from the predefined spot. Moreover, the orientations of the optic axes should be preserved to ensure accurate velocity measurements. To achieve such flexibility in the Brillouin system we divided the system into two parts (Fig. 3): the horizontal upper tier

and vertical collecting/focusing plates (which results in a vertical scattering plane). The upper tier contains the main components of the Brillouin system—Fabry-Pérot interferometer and a laser, as well as laser beam conditioning optics, part of the signal collection optics, and fixtures for aligning the optical path. Two nearly symmetric vertical plates, each mounted on two heavy-duty translation stages to the bottom of the top tier table, hold the laser focusing and signal collection optics. Thus both collection and focusing lenses can be translated along optical passes in three directions independent of each other and can deliver the focus to any spot in the vicinity of the x-ray focus. A detailed description of the setup is given below.

A. The upper tier

The upper tier is based on a $4 \times 6 \text{ ft.}^2$ optical table with an $8 \times 10 \text{ in.}^2$ rectangular hole above the typical x-ray focus position. It is mounted 40 in. above the surface of the main optical table (Fig. 3). The components of the Brillouin spectrometer include a laser, Fabry-Pérot interferometer, laser beam conditioning optics, alignment fixtures, and part of the signal transmitting optics.

We chose Coherent Verdi V2 solid-state Nd:YVO₄ frequency doubled laser with 532 nm single wavelength output. The small size of the laser head ($47 \times 11 \times 20 \text{ cm}^3$), light weight ($<10 \text{ kg}$), and very low ($<30 \text{ W}$) heat output at maximum power make it an ideal choice for the Brillouin spectrometer. The laser head is positioned on a small water-cooled heat sink, thus not noticeably affecting the temperature inside the enclosure and allows for long time uninterrupted operation of the Fabry-Pérot interferometer.

The computerized laser power supply is positioned outside the protective enclosure and is connected to a laser head with a 3 m umbilical. The output laser power and shutter can be controlled both manually from the laser power supply and remotely using standard EPICS computer interface either from inside or from outside the station.

The heart of the Brillouin spectrometer is a six-pass Sandercock-type piezoelectrically scanning tandem Fabry-Pérot interferometer TFP-1.²⁹ This is an extremely high resolution (megahertz to gigahertz range) interferometer which is intended primarily for the study of Brillouin spectra (typical frequency shift $\leq 1 \text{ cm}^{-1}$). The construction and operation of the interferometer is described in detail in Refs. 22–24. An important feature of the interferometer is that all adjustments to the interferometer optics can be made remotely from outside the interferometer enclosure.

The interferometer is dynamically stabilized in order to maintain parallel alignment of the mirrors and to correct for thermal drift of the spectrum. The stabilization is achieved by using a reference laser beam ($\sim 1 \text{ mW}$) which is picked off from the main laser beam and directed to the interferometer. Proper intensity of the reference beam is achieved by rotating a polarizing cube beam splitter, mounted inside a motorized rotational stage. This intensity is monitored by a photodiode and can be used as a feedback for dynamic control in an automatic mode.

Stabilization of the interferometer mirrors is electronically controlled with the interferometer control unit by moni-

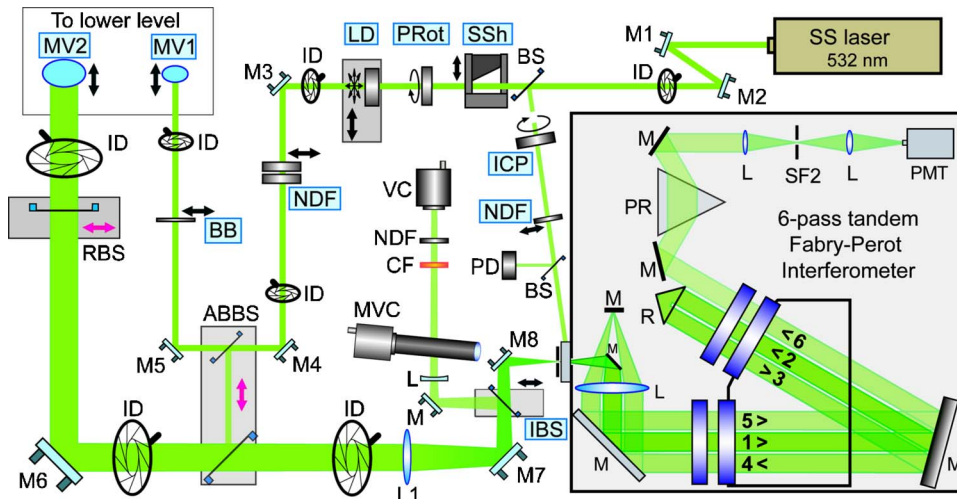


FIG. 4. (Color online) Schematic diagram of the Brillouin system—upper tier. Permanent optical elements: M, mirror; L, lens; BS, beam splitter; PR, dispersion prism; R, retroreflector; SF, spatial filter; PMT, photomultiplier tube. Laser beam/image conditioning elements: SSh, safety laser shutter; PRot, polarization rotator; LD, laser beam depolarizer; ICP, intensity control polarizer for stabilization beam; IBS, imaging beam splitter; CF, color filter; NDF, neutral density filter; BB, laser beam block. Observation/feedback elements: PD, photodiode; VC, video camera; MVC, microscope with video camera. Beam/image alignment elements: ID, iris diaphragm; ABBS, alignment beam beam splitter; RBS, retroreflecting beam splitter. All the optical elements shown with letters in boxes can be operated during run time from outside the station.

toring the intensity of the transmitted reference beam. Real time readout from the photomultiplier tube (PMT), showing the intensity of the transmitted reference light, is observed on an oscilloscope. The run-time observation of both the interferometer control unit and the oscilloscope is useful during the experiment and is monitored via a video camera that can be observed on monitors in the control area outside the experimental station.

The interferometer is equipped with a Hamamatsu 464 S PMT that provides a low dark count rate (<1 counts/s).

B. Upper tier optics

The schematic diagram of the Brillouin setup of the upper tier is shown on Fig. 4. All the components shown with boxes around the labels can be operated from the main control area outside the experimental station or any onsite networked computer. Other elements are stationary and do not require any run-time adjustment.

Before the laser beam is steered down to the bottom level toward the sample, it passes through a number of optical components that control and condition the laser beam during the experiments.

The main safety component in the beam path is an interlocked electronic shutter [safety laser shutter (SSh)]. It prevents the laser beam from leaving the top tier and prevents the potentially dangerous exposure of people to an open laser beam. The shutter closes automatically during any unsafe operations, or it can be closed remotely as needed. The shutter is positioned after the beam splitter (BS) which picks off the reference beam for stabilization. Therefore even when the shutter is closed, the stabilization of the interferometer is preserved, eliminating the need for a potentially lengthy re-stabilization procedure.

Correct polarization of the input beam can be critical for obtaining the optimal Brillouin signal. Therefore the polarization of the laser beam can be controlled remotely by a half-wave plate [polarization rotator (PRot)]. When the optimal polarization is not known *a priori*, the linear polarization of laser light can be transformed into circular polarization

with a removable first-order quarter wave plate [laser beam depolarizer (LD)].

An observation of the laser focus on the sample is performed by video cameras. Two neutral density filters are used to attenuate the laser power and allow for easier focusing and aligning the laser beam on the sample.

Our system uses a split collection path for different scattering geometries. Therefore all the collecting optics are aligned with respect to a reference beam, which is picked off from the main laser beam and introduced into the collecting path in its middle with two pellicle beam splitters [alignment beam beam splitter (ABBS)] and a retroreflector [retroreflecting beam splitter (RBS)].

The sample image, containing inelastically scattered light, is projected onto the entrance pinhole of the interferometer. The image on the pinhole is observed with microscope equipped with a video camera (MVC) and a long focal distance objective. A fraction of the image light can be picked off with a pellicle imaging beam splitter (IBS), conditioned with a neutral density and a color filter, and focused directly onto a charge coupled device (CCD) chip of an additional video camera, thus providing a higher resolution with a better quality image.

C. Focusing/collecting optics

The sample position on the lift table is determined by the position of the focused x-ray beam which cannot be readily changed without lengthy realignment. Thus, simultaneous Brillouin and x-ray measurements require that focusing and collecting optics of the Brillouin system can move easily with respect to the sample to bring both the laser focus and collecting spot to a predetermined point. The critical consideration for Brillouin spectroscopy is that during such movement all the angular relations in the system should be preserved (to provide a correct scattering angle and phonon direction), and that the collected scattered light should enter the Fabry-Pérot interferometer along its optical axis to prevent loss of signal.

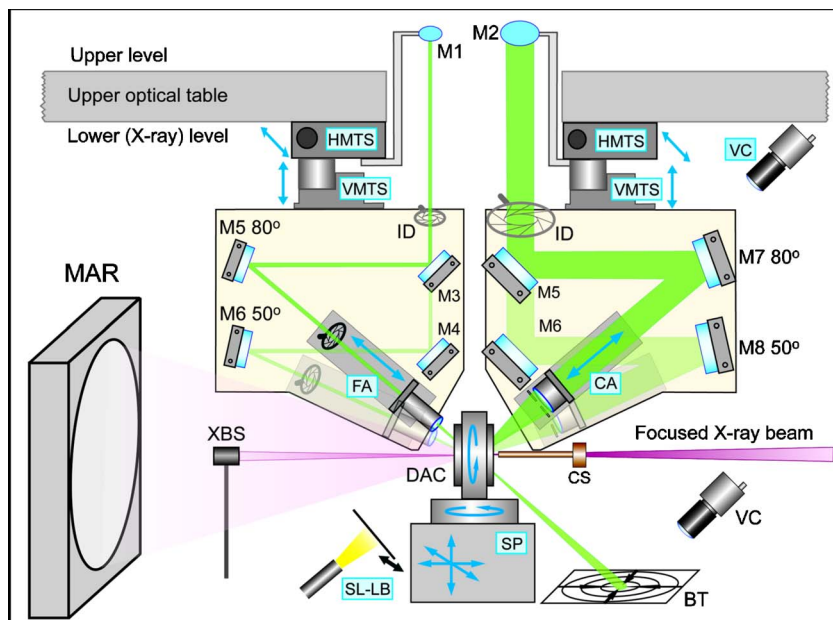


FIG. 5. (Color online) Schematic diagram of the lower tier of the combined Brillouin–x-ray system. Motorized translation components (fully controllable from outside the hatch, shown in boxes): HMTS, horizontal motorized translation stage; VMTS, vertical motorized translation stage; FA, motorized laser focusing assembly; CA, motorized signal collecting assembly; SP, sample positioning and orientation assembly; SL-LB, sample light/light block. Observation/feedback elements (red boxes): VC, video camera; BT, beam target. X-ray components: MAR, MAR345 imaging plate; XBS, x-ray beam stop; CS, cleanup slit.

The optical components along the focusing/collecting paths of the spectrometer can translate independently to satisfy these requirements (Fig. 5 and 6). These optics (lenses and mirrors) are mounted on symmetric aluminum platforms that are attached to heavy-duty linear translation stages, allowing the platforms to move in the vertical and horizontal directions (parallel to the optic axes of the Brillouin system and perpendicular to the x-ray beam). In between measurements the platforms can be raised by ~ 15 cm for easy sample replacement and alignment. Each platform has two sets of mirrors for 80° and 50° scattering geometry. One mirror on each platform (M3 and M5) is mounted on a flip mount so that the optical path can be easily switched between 80° and 50° geometries.

For focusing the laser beam we use a long focal distance (50 or 75 mm) microscope objective. The lens is mounted on a linear translation stage. Such a focusing assembly can be kinematically mounted on a platform in one of two predefined positions for either 50° or 80° scattering.

The collecting platform has a nearly symmetric configuration, except with mirrors larger than used for the incident light. For signal collection we use an achromatic lens with 30 mm diameter and 100 mm focal length. An aperture mask (2.5–5 mm wide slit, vertical with respect to the scattering plane) is used to reduce the astigmatism caused by the inclined diamonds and decrease the range of scattering angles. This increases the sharpness and signal-to-noise ratio, thus increasing resolution and quality of the Brillouin spectra.

Two mirrors, postmounted to heavy-duty horizontal translation stages, protrude through the opening in the upper tier table and turn the laser along the upper collecting path.

V. LASER SAFETY

The Coherent Verdi V2 diode laser used for Brillouin experiments can produce up to a 2 W of output laser power and therefore is a class 4 laser, which represents a hazard for eye damage from the direct beam, specular reflections, and possibly diffuse reflections. Therefore, the interior of the 13

BM-D station is a laser controlled area (LCA) and special measures must be taken to ensure safe working conditions.

The laser and all active system components are remotely controlled by a computer interface from the 13 BM-D control area. The presence of a user inside the station for performing experiments (except for positioning the sample) is not required.

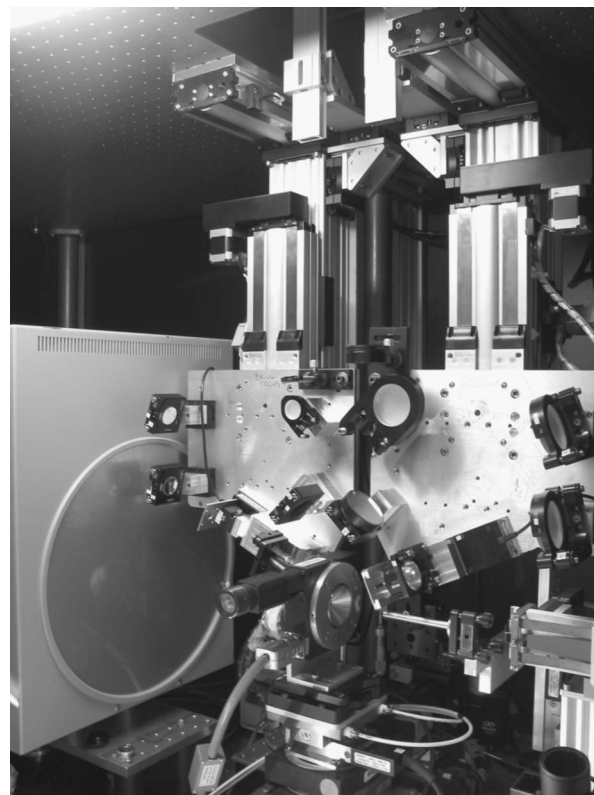


FIG. 6. The lower tier of the combined Brillouin–x-ray system. On the current photograph the system is ready for simultaneous Brillouin (50° geometry) and x-ray (with MAR345 imaging plate) measurements. The sample is positioned in a motorized rotation stage perpendicular to focused x-ray beam.

An interlocked enclosure completely surrounds the laser setup and laser beam path during normal operation. The enclosure consists of stationary and removable solid laser shielding panels mounted on an aluminum frame. The top tier has a permanent enclosure which can be opened only during the optics alignment, performed only by authorized personnel. The lower tier has an enclosure made of removable panels, which must be in place during experiments involving lasers and can be removed during other experiments. The experimental station is equipped with a complex interlock system which is used to prevent operation of the lasers in an unsafe condition and exposure to the laser beam. It is designed to allow access to the laser beam only for authorized users for optics alignment. The interlock system is designed in such a way that if fault condition occurs, the external shutter system will block the beam from entering the lower level, while the stabilization beam to the interferometer will remain on and the stabilized state will not be disrupted. This allows one to perform manual operations with the sample (positioning and removing, adjusting manual rotation stages, etc.) on the bottom level without being exposed to laser light and without interrupting the stabilized state of the interferometer. An attempt to access the optical components on the top tier while the laser beam is present would close the main laser shutter and thus cause the interferometer to lose stabilization.

VI. EXPERIMENTS

Below we provide a short description of advantages and downsides of both single crystal and polycrystalline Brillouin measurements and show examples of measurements performed during the commissioning of the system.

A. Single crystal measurements

The described Brillouin system is ideally suited for measuring single crystal elastic moduli of materials in DAC. In the current symmetric configuration the direction of a measured phonon is vertical. Thus by rotating the symmetrical DAC around its horizontal axis, which is perpendicular to the sample plane, the velocities in any crystallographic direction within the sample plane can be easily measured (Fig. 2).

The combination of the x-ray and Brillouin measurements has a number of advantages for single crystal elasticity studies. First, the orientation of the sample and especially the phonon direction can be determined unambiguously from a diffraction image. Second, the stress state of the crystal and its deformation (mosaic spread) can be assessed from analysis of the diffraction image and integrated spectra. Third, the single crystal x-ray diffraction measurements are an order of magnitude faster than those on polycrystalline samples due to spatial concentration of diffracted energy, with typical exposure time for our samples in the range of 15–30 s. Fourth, the lattice parameters can be easily determined, especially in high symmetry materials and samples with zone axis orientation. For example, in the case of MgO and NaCl, rotating the diamond cell with a sample around a vertical axis by $\pm 10^\circ$ produces four to six individual diffraction reflections (at 37 keV with 350 mm diameter imaging plate), which al-

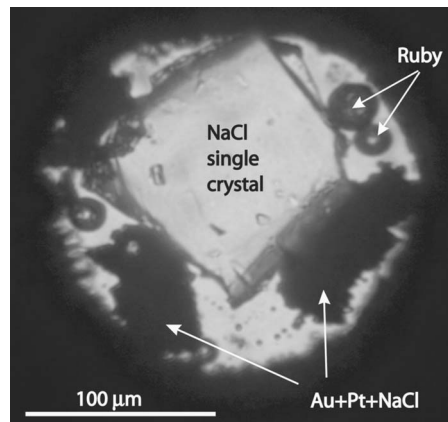


FIG. 7. Single crystal NaCl (B1) in DAC loaded with Ne at 26 GPa. Ruby and a mixture of Au, Pt, and powdered NaCl are loaded as pressure calibrants.

lows accurate lattice parameter determination. The single crystal diffraction images can be indexed and processed the same ways as polycrystalline spectra using the standard image-processing software [e.g., ESRF FIT2D (Ref. 25)].

As an example here we present the results of Brillouin and x-ray measurements on a single crystal of NaCl at 26 GPa. A cleaved plate of single crystal NaCl was loaded into DAC with Ne as a hydrostatic pressure medium. Ruby balls²⁶ and a mixture of Au, Pt, and NaCl powder were added to the sample chamber for pressure estimation and cross calibration (Fig. 7). The DAC was mounted in a motorized rotational stage and the sample was preoriented with the [100] direction facing up. The diffraction image (Fig. 8) shows four sets of individual x-ray reflections [(200), (220), (400), and (420)]. The almost round shape of the reflections indicates the absence of any significant deviatoric stress on the sample. From this image the orientation of the single crystal sample can be easily obtained. The x-ray image was integrated using a polycrystalline routine in the FIT2D program. 2θ -intensity plot (Fig. 9) shows extremely sharp and well defined diffraction peaks.

A typical Brillouin spectrum is shown on Fig. 10. De-

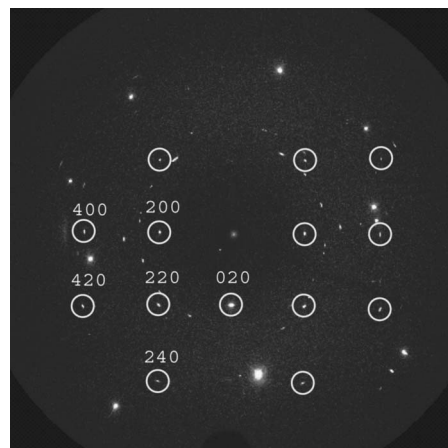


FIG. 8. X-ray diffraction image of single crystal NaCl (B1) at 26 GPa with Ne as a pressure medium. Single crystal diffraction spots of NaCl are shown in circles. The sample was rotated around the vertical ω axis by $\pm 10^\circ$ during the x-ray exposure.

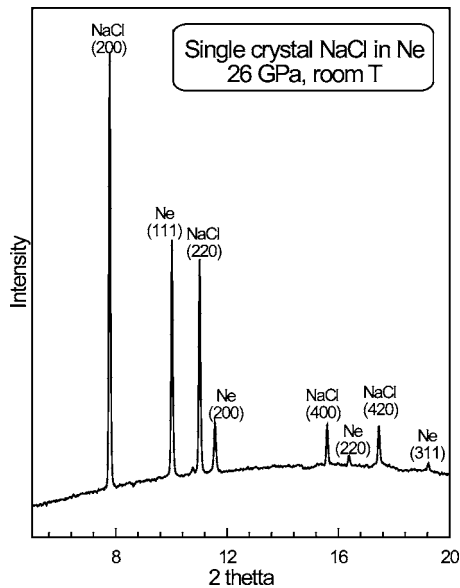


FIG. 9. Integrated x-ray diffraction pattern on single crystal NaCl and polycrystalline Ne at 26 GPa and room temperature.

spite a relatively high background due to elastic scattering of laser light from metal powder, the Brillouin peaks of NaCl are sharp and well defined, thus providing unambiguous velocities. NaCl has a simple cubic structure ($Fm\bar{3}m$) and its elasticity is completely characterized by three independent elastic moduli. Thus, velocity measurements in two distinct crystallographic directions would be sufficient to completely characterize its elasticity tensor and calculate aggregate elastic moduli (adiabatic bulk and shear moduli) and acoustic velocities. Nevertheless we measured the acoustic velocities in four well defined crystallographic directions ($[100]$, $[110]$, and intermediate directions) to increase the accuracy of the elastic moduli (Fig. 11). The velocity and density were used to calculate single crystal elastic moduli, and the velocities calculated from the best fit elastic constants are shown by the lines on Fig. 11.

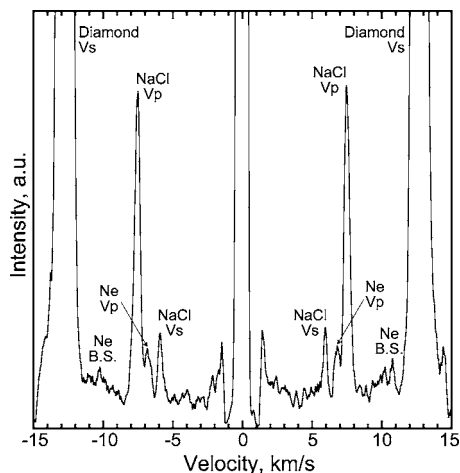


FIG. 10. Single crystal Brillouin spectrum of NaCl ($B1$ phase) in the $[110]$ direction at 26 GPa. The crystal is loaded into a diamond cell with neon pressure medium. Ne BS, backscattering peak(s) of neon.

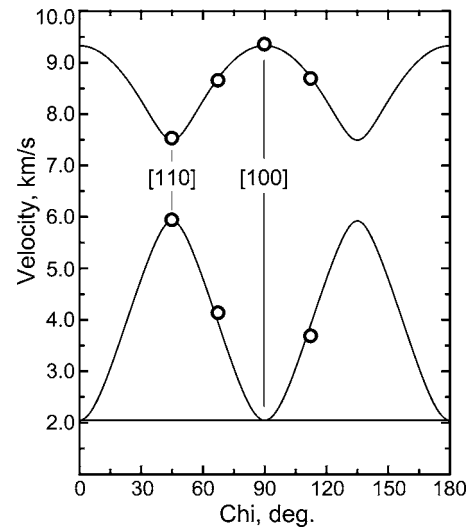


FIG. 11. Acoustic velocities of NaCl at 26 GPa as a function of crystallographic direction. Circles—measured velocities. Lines—velocities calculated from the best fit single crystal elastic moduli.

B. Measurements on polycrystalline samples

In single crystal x-ray diffraction with a monochromatic x-ray beam and a stationary area detector the sample must be rotated around at least one axis not coincident with the x-ray beam to obtain a representative x-ray image. This makes truly simultaneous collection of the Brillouin and x-ray diffraction measurements problematic. On the other hand, x-ray powder diffraction can be easily performed on a stationary sample. Thus the use of polycrystalline samples provides an excellent opportunity for simultaneous Brillouin and acoustic velocity measurements from the same volume of the sample. Because the collecting optics of the Brillouin system has an in-line observation system, the laser and x-ray beam focuses can be easily aligned using either visible fluorescence of ruby excited by an x-ray beam or the sharp edges of a gasket hole.

The advantage of measurements on polycrystalline samples is that the angle-dispersive x rays provide a direct measurement of lattice parameters (and hence the density of the sample) while simultaneous Brillouin measurements provide a direct measurement of the aggregate compressional (V_p) and shear (V_s) velocities. From the density and aggregate velocities the adiabatic bulk [$K_S = \rho V_p^2 - (4/3)V_s^2$] and shear ($\mu = \rho V_s^2$) moduli are readily calculated. Nevertheless, Brillouin scattering on polycrystalline materials has several drawbacks as compared to single crystal measurements.

The quality and accuracy of polycrystalline Brillouin measurements critically depend on the elastic anisotropy of the studied material. If the acoustic anisotropy of a material is too high, the Brillouin peaks are broad and determination of an aggregate velocity from the peak position is somewhat ambiguous or even impossible (e.g., NaCl in the $B1$ phase at pressures above 20 GPa, where the maximum V_s velocity is three times faster than the minimum). Another anisotropy-related factor is the intensity of Brillouin peaks. In anisotropic materials the Brillouin frequencies are spread over some finite range, and the volume of material contributing to a given Brillouin frequency is small. Thus, collecting a Brillouin

louis spectrum from a polycrystalline sample can take significantly more time to obtain an adequate signal-to-noise ratio. In addition, the grain boundaries in polycrystalline samples tend to generate a significant amount of elastic scattering (noise) which is seen in the spectra as a high background, thus further decreasing signal-to-noise ratio and increasing collection time.

Additional complications can be introduced if not enough care is taken to keep the uniform (hydrostatic) stress conditions in the diamond cell, which can, in addition to stress-related artificial anisotropy, cause the development of preferred orientation in crystallites, thus jeopardizing the quality and accuracy of Brillouin measurements.

Nevertheless, in many cases polycrystalline Brillouin measurements can be much more advantageous than single crystal measurements. A beneficial fact is that in many minerals (with a few exemptions) the elastic anisotropy decreases with pressure [e.g., MgO (Refs. 12 and 27 ringwoodite²⁸), thus making the polycrystalline Brillouin measurements at high pressures more reliable.

Furthermore, unquenchable phases and many extremely high-pressure phases [e.g., Ca perovskite, postperovskite phase of (Mg,Fe,Al)(Si,Al)O₃, and high-pressure phases of alkali halides] simply cannot be obtained in single crystals and their elastic property measurements can only be performed on polycrystalline aggregates.

Our earlier measurements showed that for minerals with low or moderate acoustic anisotropy [e.g., garnets^{12,14,19} or MgSiO₃ perovskite¹⁵) the directly measured aggregate acoustic velocities, and hence the aggregate elastic moduli, are identical (within the experimental uncertainties) to those calculated from well-resolved single crystal elastic moduli.

Perhaps the greatest benefit comes when the high-pressure measurements are performed at high temperature, especially with laser heating. In this case it is highly beneficial to perform simultaneous x-ray and Brillouin measurements from the same spot of the sample, which is problematic with single crystals. This can minimize the effect of pressure drifting in the time between x-ray and Brillouin measurements and eliminates the necessity to measure several crystallographic directions.

As an example of experiments on a polycrystalline sample, we show the results of experiments on a polycrystalline sample of NaCl in *B2* phase at 35 GPa. Powdered NaCl was loaded into a Merrill-Bassett-type diamond cell modified for Brillouin scattering with large aperture openings together with pieces of CaSiO₃ glass as well as ruby chips and gold flakes for pressure measurements. The pressure was increased until NaCl transformed from the *B1* to the *B2* phase. Before the measurements the sample was annealed with a CO₂ laser (which coupled with silicate glass and ruby). Pressure was first measured by a ruby fluorescence technique⁴ and then confirmed by measuring lattice parameters of gold powder. The x-ray spectrum also shows remnants of untransformed *B1* phase of NaCl (<2%) which was also used to constrain the pressure. The focused x-ray beam ($\sim 7 \times 20 \mu\text{m}^2$) and laser focus ($\sim 15 \times 15 \mu\text{m}^2$) have comparable sizes. The laser and x-ray beam focuses were coaligned using sharp edges

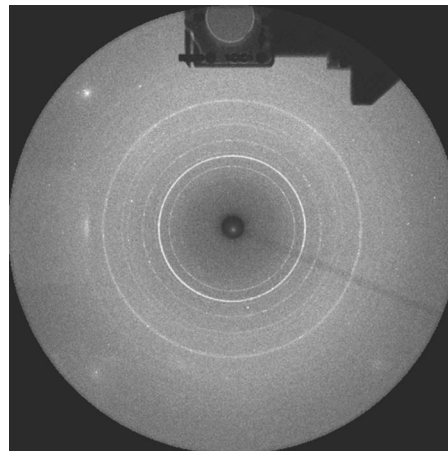


FIG. 12. MAR 345 detector image of polycrystalline NaCl in *B2* phase at 35 GPa. The x-ray image was collected simultaneously with the Brillouin spectra. The shade on the top portion of the image is from focusing optics of the Brillouin system.

of the gasket hole. The x-ray image (Fig. 12) and polycrystalline Brillouin spectrum (Fig. 13) were collected simultaneously from the same spot in the sample. The uniform distribution of diffraction rings indicates that there is no significant preferred orientation in the sample. The Brillouin and x-ray diffraction peaks are sharp, indicating a small stress gradient across the sample. The sharp Brillouin peaks also show low elastic anisotropy of *B2* NaCl at this pressure. The measured aggregate acoustic velocities and density were used to calculate isotropic adiabatic bulk (K_S) and shear (μ) moduli from a single Brillouin and x-ray exposure.

C. Measurements at high temperature

The pilot single crystal Brillouin and angle-dispersive x-ray measurements on MgO were performed at simultaneous high pressure and temperature (to 600 °C) in a resistively heated DAC. The DAC was of the Merrill-Bassett type modified with large openings for Brillouin velocity measurements. The resistive heater consisted of a platinum wire wound on a ring-shaped ceramic template. The temperature

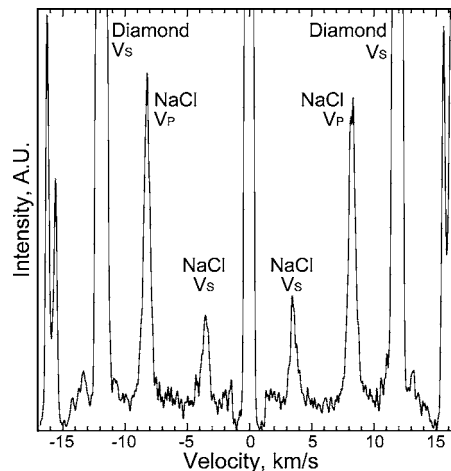


FIG. 13. Brillouin spectrum of polycrystalline NaCl in *B2* structure at 35 GPa collected simultaneously with x-ray diffraction image shown on Fig. 12.

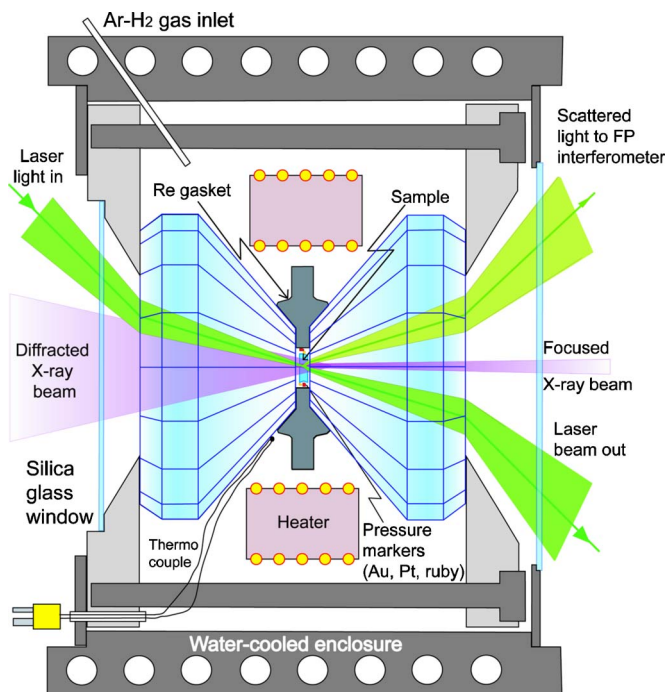


FIG. 14. (Color online) Schematic diagram of an externally heated DAC for Brillouin and x-ray diffraction measurements in a water-cooled gas-tight enclosure.

was controlled by two thermocouples (*K* and *R* types) attached to opposite sides of the diamond with a high-temperature cement close to the culet. The difference in temperature readings from the *K* and *R* thermocouples was within 1 K. The heater was powered by a 33 V-33 A remotely controllable dc power supply. The temperature was controlled by a feedback loop to within a fraction of a degree.

To protect the diamonds and tungsten carbide seats from disintegration and oxidation the cell was mounted inside a water-cooled enclosure with additional 150 μm thick silica glass windows and a flow of reducing Ar-2% H₂ mixture (Fig. 14). The enclosure with the DAC was mounted inside a manual rotation stage (with the rotation axis along the x-ray beam) to vary the sampled phonon direction.

A single crystal of MgO polished into a platelet of $\sim 15 \mu\text{m}$ thickness with (100) orientation was cryogenically loaded with Ar as a pressure medium. Ruby chips as well as gold and platinum powder were added to the sample chamber as pressure standards. The pressure in the DAC was set at room temperature, and then the temperature was increased in 150 $^{\circ}\text{C}$ increments. Due to relaxation of the DAC, the pressure decreased appreciably as the temperature increased. Nevertheless, after temperature stabilization, the pressure inside the DAC also stabilized. X-ray measurements were performed before and after Brillouin measurements to confirm pressure stability. While Ar was solid, the pressure remained constant throughout the experiments at the same temperature. When Ar melted, some pressure drift was observed. A typical Brillouin spectrum is shown on Fig. 15.

ACKNOWLEDGMENTS

The authors thank GSECARS staff Fred Sopron, Mike Jagger, and Nancy Lazars who provided invaluable support

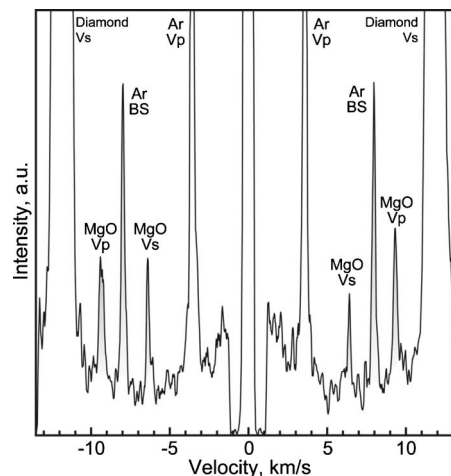


FIG. 15. Brillouin spectrum of MgO at 8 GPa and 600 $^{\circ}\text{C}$. At these conditions Ar is in liquid state and shows only V_P and backscattering (Ar BS) peaks.

for this program. This work was supported by COMPRES and the National Science Foundation. GeoSoilEnviroCARS [Sector 13, Advanced Photon Source (APS), Argonne National Laboratory] is supported by the National Science Foundation—Earth Sciences (EAR-0217473), Department of Energy—Geosciences (DE-FG02-94ER14466), and the State of Illinois. Use of the Advanced Photon Source was supported by the U.S. Department of Energy, Office of Science, Office of Basic Energy Sciences, under Contract No. W-31-109-ENG-38.

- ¹ S. R. Shieh, T. S. Duffy, A. Kubo, G. Shen, V. B. Prakapenka, N. Sata, K. Hirose, and Y. Ohishi, *Proc. Natl. Acad. Sci. U.S.A.* **103**, 3041 (2006).
- ² S. D. Jacobsen, J. F. Lin, R. J. Angel, G. Shen, V. B. Prakapenka, P. Dera, H.-K. Mao, and R. J. Hemley, *J. Synchrotron Radiat.* **12**, 577 (2005).
- ³ M. Murakami, S. V. Sinogeikin, H. Hellwig, and J. D. Bass, *Earth Planet. Sci. Lett.* (submitted).
- ⁴ H. K. Mao, P. M. Bell, J. W. Shaner, and D. J. Steinberg, *J. Appl. Phys.* **49**, 3276 (1978).
- ⁵ A. L. Ruoff, R. C. Linkoln, and Y. C. Chen, *J. Phys. D* **6**, 1295 (1973).
- ⁶ B. S. Li, J. Kung, T. Uchida, and Y. B. Wang, *J. Appl. Phys.* **98**, 013521 (2005).
- ⁷ H. J. Mueller, F. R. Schilling, J. Lauterjung, and C. Lathe, *Eur. J. Mineral.* **15**, 865 (2003).
- ⁸ S. V. Sinogeikin, D. L. Lakshtanov, J. D. Nicholas, and J. D. Bass, *Phys. Earth Planet. Inter.* **143-144**, 575 (2004).
- ⁹ S. V. Sinogeikin, J. D. Bass, and T. Katsura, *Phys. Earth Planet. Inter.* **136**, 41 (2003).
- ¹⁰ G. B. Benedek and K. Fritsch, *Phys. Rev.* **149**, 647 (1966).
- ¹¹ C.-S. Zha, T. S. Duffy, R. T. Downs, H.-K. Mao, and R. J. Hemley, *J. Geophys. Res.* **101**, 17 (1996).
- ¹² S. V. Sinogeikin and J. D. Bass, *Phys. Earth Planet. Inter.* **120**, 43 (2000).
- ¹³ C. H. Whitfield, E. M. Brody, and W. A. Bassett, *Rev. Sci. Instrum.* **47**, 942 (1976).
- ¹⁴ S. V. Sinogeikin and J. D. Bass, *Geophys. Res. Lett.* **29**, 4-1 (2002).
- ¹⁵ S. V. Sinogeikin, J. Zhang, and J. D. Bass, *Geophys. Res. Lett.* **31**, L06620 (2004).
- ¹⁶ A. E. H. Love, *A Treatise on the Mathematical Theory of Elasticity* (Dover, New York, 1944).
- ¹⁷ D. J. Weidner and H. R. Carleton, *J. Geophys. Res.* **82**, 1334 (1977).
- ¹⁸ G. Shen, V. B. Prakapenka, P. J. Eng, M. L. Rivers, and S. R. Sutton, *J. Synchrotron Radiat.* **12**, 642 (2005).
- ¹⁹ J. D. Bass, *J. Geophys. Res.* **84**, 7621 (1989).
- ²⁰ S. Speziale and T. S. Duffy, *Phys. Chem. Miner.* **29**, 465 (2002).
- ²¹ S. V. Sinogeikin, T. Katsura, and J. D. Bass, *J. Geophys. Res.* **103**, 20 (1998).
- ²² J. R. Sandercock, in *Light Scattering in Solids III*, Topics in Applied

- Physics Vol. 51, edited by M. Cadona and G. Guntherodt (Springer, Berlin, 1982), p. 173.
- ²³R. Mock, B. Hillebrands, and J. R. Sandercock, *Rev. Sci. Instrum.* **20**, 656 (1987).
- ²⁴S. M. Lindsay, M. W. Anderson, and J. R. Sandercock, *Rev. Sci. Instrum.* **52**, 1478 (1981).
- ²⁵A. P. Hammersley, S. O. Svensson, M. Hanfland, A. N. Fitch, and D. Hausermann, *High Press. Res.* **14**, 235 (1996).
- ²⁶J. C. Chervin, B. Canny, and M. Mancinelli, *High Press. Res.* **21**, 305 (2001).
- ²⁷C.-S. Zha, H.-K. Mao, and R. J. Hemley, *Proc. Natl. Acad. Sci. U.S.A.* **97**, 13 (2000).
- ²⁸S. V. Sinogeikin, J. D. Bass, and T. Katsura, *Geophys. Res. Lett.* **28**, 4335 (2001).
- ²⁹www.jrs-si.com